Multi-phase flow of Jeffrey Fluid bounded within magnetized horizontal surface

Mubbashar Nazeer [a], Farooq Hussain [b], M. Ozair Ahmad [c], Sadia Saeed [c], M. Ijaz Khan [d], Seifedine Kadry [e], Yu-Ming Chu [f,g,*]

[a] *Department of Mathematics, Institute of Arts and Sciences, Government College University Faisalabad, Chiniot Campus 35400, Pakistan*
[b] *Department of Mathematical Sciences (FABS) BUITEMS, Quetta 87300, Pakistan*
[c] *Department of Mathematic, The University of Lahore, Lahore 54890, Pakistan*
[d] *Department of Mathematic and Statistics, Riphah International University I-14, Islamabad 44000, Pakistan*
[e] *Department of Mathematics and Computer Science, Beirut Arab University, Beirut, Lebanon*
[f] *Department of Mathematics, Huzhou University, Huzhou 313000, PR China*
[g] *Hunan Provincial Key Laboratory of Mathematical Modeling and Analysis in Engineering, Changsha University of Science & Technology, Changsha 410114, PR China*

ARTICLE INFO

ABSTRACT

Present communication explores the multi-phase flow of non-Newtonian fluid with heat transfer through a horizontal channel. Jeffrey fluid is considered as the base liquid which suspends metallic particles of Hafnium (*Hf*). Heating effects have been applied on the upper wall. The magnetic field, along with radiative heat flux, has also been taken into account. Three different particulate flows, namely; (i) pressure-driven multi-phase flow, (ii) moving wall-driven multi-phase flow and, (iii) pressure and moving wall driven multi-phase, are derived. A closed-form solution for each bi-phase flow is achieved and compared. The impacts of most significant emerging parameters, on velocity and temperature profile, are observed graphically. It is inferred that more thermal energy adds to the system friction force and viscous dissipation, whereas, heat transfer rate increases due to radiation. The momentum of multi-phase flow enhances due to shear thinning effects caused by Jeffrey fluid parameter.

1. Introduction

Non-Newtonian fluids are always problematic to be predicted with the help of Navier Stokes equations, because of extremely non-linear relation between applied stresses and strain. Some familiar examples of such fluids are oils and paints, blood, gels, and adhesives etc. Several mathematical models have been derived to analyze such complex fluids and, Jeffrey fluid model is one of such fluids. It is a famous viscoelastic non-Newtonian fluid, which helps explain the performance of retardation and relaxation times. There are two parameters $\widehat{\lambda}_1$ and $\widehat{\lambda}_2$ in Jeffery fluid tensor in which $\widehat{\lambda}_1$ describes retardation time and $\widehat{\lambda}_2$ is a ratio between retardation time to relaxation time. Because of viscoelastic properties, Jeffrey fluid has numerous applications in polymer productions. The exclusive uses of Jeffrey fluid in industries seek the intention of researchers; that's why many studies based on different geometries of Jeffrey fluid have been presented from the last few decades [1–5].

Ramesh [6] investigated the Jeffrey fluid and pointed out the joule heating and viscous dissipation effects. He discussed plane Couette flow, generalized Couette flow, and plane Poiseuille flow and presented the exact solution under the impact of boundary slip conditions. The MHD Jeffrey nanofluid examined by Abbasi et al. [7]. The result of this study revealed that Jeffrey fluid model gives large values of Sherwood and Nusselt numbers than the viscous fluid. The effects of heat generation and thermal radiation on the hydromagnetic 3-D flow of Jeffrey fluid explored by Shehzad et al. [8]. They picked the homotopy analysis method to solve governing equations and interpret the impacts of all concerned parameters. Turkyilmazoglu and Pop [9] presented the analytical solutions for mass and heat transmission of Jeffrey fluid. They concluded that the Prandtl number affects the temperature distribution, and Deborah's number affects flow distribution. Ellahi et al. [10,11] have obtained exact, and closed-form solutions for Jeffrey fluid flow. Nano flow is analyzed in a catheterized tapered artery while a rectangular duct is used for the peristaltic transport of Jeffrey fluid. The results interpreted that the thermal radiation parameter accelerates the temperature of the liquid and also increases boundary layer thickness.

Multi-phase flows of Newtonian and non-Newtonian fluids are of

---

Nomenclature

$\widehat{h}$	Distance between plates
$\widehat{T}_0$	Lower plate temperature
$\widehat{\lambda}_1, \widehat{\lambda}_2$	Jeffrey fluid parameters
$\widehat{M}$	Hartmann number
$\dot{\gamma}$	Deformation tensor
$\widehat{u_f}$	The dimensional velocity of fluid phase
u_f^*	The dimensionless fluid phase velocity component
$\widehat{\mu_s}$	Dimensional viscosity of the solid-liquid
$\widehat{T}$	The dimensional temperature of the fluid
$\widehat{p}$	Dimensionless pressure gradient parameter
$\widehat{B_r}$	Brinkman number
$\overline{\mu}$	The viscosity of the base liquid
$\widehat{\sigma}$	Electrical conductivity
$\widehat{C}$	Concentration of particles
U	Velocity of moving wall
$\widehat{\mathbf{B}}$	Total Magnetic field
$\widehat{T}_1$	Upper plate temperature
$\widehat{\rho_f}$	Density of fluid
$\widehat{\mathbf{s}}$	Jeffrey stress tensor
$\ddot{\gamma}$	Substantial derivative
$\widehat{u_p}$	The dimensional velocity of particle phase
u_p^*	The dimensionless particle-phase velocity component
μ_s^*	Dimensionless viscosity of Fluid
T^*	The dimensionless temperature of the fluid
$\widehat{C_p}$	Specific heat
$\widehat{R_d}$	Radiation parameter
$\widehat{s}$	Coefficient of drag force exerted by particles
B_0	Magnetic strength
k^*	Dimensionless thermal conductivity
S	Drag coefficient

great significance. Many natural flows are solely a liquid flow but comprise different kinds of solid or air particles. The most common natural flows are floods, avalanche and granular flows etc. Mubbashar et al. [12] is a comparative study of non-Newtonian multi-phase flows. Fourth-grade fluid model is used to make suspension with Hafnium and crystal particles. Supercritical flows are investigated and compared. Zeeshan et al. [13] considered tiny for the two-dimensional flow of Couples stress fluid over a paraboloid of revolution. The heat and mass transfer through the base liquid is investigated numerically. Ellahi et al. [14] examined the two-phase Couette flow of Couple stress fluid. Uniform magnetic field is applied, which hinders the flow Hafnium suspended flow. Zeeshan et al. [15] analyzed the gravity-driven flow of Couple stress fluid. Closed-form solutions are obtained for Magnetohydrodynamic (MHD) of bi-phase flows. Similarly, in [16] authors have presented analytical solutions for two different types of multi-phase flow. They used a regular perturbation method to explore the flow dynamics of Third-grade bi-phase flows.

Heat and mass transfer is a vital mechanical phenomenon. The transmission properties of heat and mass transfer through tangent hyperbolic nanofluid are discussed by Atif et al. [17]. Peristaltic transport to Rabinowitsch fluid with heat transfer incorporated with radiative heat flux is reported by Chu et al. [18]. Flow is generated by the walls furnished with cilia structure while the thermal effects attenuate the liquid's viscosity. A numerical scheme is taken into account for the non-linear differential equations subject to convective boundary conditions. Numerical and analytical solutions are obtained and compared for Third grade fluid in [19]. Heat transfer is investigated through a porous channel by using thermal and velocity slip conditions. Numerical simulation is carried out by Ellahi et al. for two-phase flow in [20]. Lubrication effects are employed on the wall to reduce the roughness of the surface. Bhatti et al. [21] investigated the heat transfer effects during motion of solid particles through the channel. They have used the shooting technique to solve the complex non-linear problem. They presented their solutions by sketching graphs for temperature and velocity fields. Some more work related to the current study can be seen by Ref [22–28].

Three fundamental bi-phase flows of excellent mechanical and industrial significance are addressed in this article. Jeffrey fluid suspended with metallic particles have not been reported, yet in the existing literature. In addition to this, heat transfer with the contribution of radiation on multi-phase flow is theoretically modeled, for the first time.

2. Mathematical analysis

Consider a two-phase flow of non-Newtonian fluid with heat transfer in a horizontal channel. Jeffrey fluid is considered as the base liquid suspended with metallic Hafnium particles. A uniform magnetic field is applied in the transverse direction of the walls which are $\widehat{k} = \pm\widehat{h}$ distance away from each other. The lower and upper plates of the channel are maintained at a temperature $\widehat{T}_0$ and $\widehat{T}_1$, respectively.

Let $\widehat{\mathbf{V}}_{\widehat{f}} = (0, \widehat{u_f}(\widehat{k}), 0)$, $\widehat{\mathbf{V}}_{\widehat{p}} = (0, \widehat{u_p}(\widehat{k}), 0)$ be the fluid phase and the particle phase velocities, respectively for an MHD two-phase flow with the contribution of radiative heat flux. Then the set of equations for an MHD heated two-phase Jeffrey-Hafnium flow are given as:

2.1. Fluid phase equations

Equations for the conservation of mass for the fluid phase is

$$\nabla . \widehat{\mathbf{V}}_{\widehat{f}} = 0. \tag{1}$$

Conservation of linear momentum the fluid phase is

$$-\left(1 - \widehat{C}\right)\nabla\widehat{p} + \left(1 - \widehat{C}\right)\nabla.\widehat{\mathbf{s}} - \widehat{s}\widehat{C}\left(\widehat{\mathbf{V}}_{\widehat{p}} - \widehat{\mathbf{V}}_{\widehat{f}}\right) + \widehat{\mathbf{J}} \times \widehat{\mathbf{B}}$$
$$= \widehat{\rho_f}\left(1 - \widehat{C}\right)\frac{D\widehat{\mathbf{V}}_{\widehat{f}}}{D\widehat{t}}. \tag{2}$$

2.2. Particle phase equations

Equations for Conservation of mass is

$$\nabla . \widehat{\mathbf{V}}_{\widehat{p}} = 0. \tag{3}$$

The equation for the linear momentum of particle-phase [29] is

$$\widehat{\rho_{\widehat{p}}}\widehat{C}\frac{D\widehat{\mathbf{V}}_{\widehat{p}}}{D\widehat{t}} = -\widehat{C}\nabla\widehat{p} + \widehat{S}\widehat{C}\left(\widehat{\mathbf{V}}_{\widehat{p}} - \widehat{\mathbf{V}}_{\widehat{f}}\right). \tag{4}$$

2.3. Heat transfer equation

The equation which describes the heat transfer of the multi-phase flow of Jeffrey fluid incorporated with thermal radiation effects is given as

$$\widehat{\rho}_f\left(\widehat{C}_{\widehat{p}}\right)_f \frac{D\widehat{T}}{D\widehat{t}} = \nabla \cdot \widehat{k}\nabla\widehat{T} + \widehat{\mu}_s\widehat{\phi} - \frac{\widehat{q}_{\widehat{r}}}{\partial\widehat{k}}, \tag{5}$$

In above one can identify $\widehat{\phi} = tr(\widehat{\mathbf{s}} \cdot \mathbf{L}^\frown)$. Here, $\widehat{\mathbf{s}}$ as extra stress tensor for the Jeffrey fluid and **L** is Rivlin-Ericksen tensor

$$\widehat{\mathbf{s}} = \frac{\widehat{\mu}_s}{1+\widehat{\lambda}_1}\left(\dot{\gamma} + \widehat{\lambda}_2\ddot{\gamma}\right). \tag{6}$$

The deformation tensor $\dot{\gamma}$ and substantial derivative $\ddot{\gamma}$ are given by

$$\dot{\gamma} = \mathbf{L}^\frown + \mathbf{L}^\frown \widehat{\mathbf{T}}. \tag{7}$$

$$\ddot{\gamma} = \frac{d\dot{\gamma}}{d\widehat{t}} = \frac{\partial\dot{\gamma}}{\partial\widehat{t}} + \left(\widehat{\mathbf{V}}\cdot\nabla\right)\dot{\gamma}. \tag{8}$$

With the assumption of unidimensional flow, it is obtained

$$\mathbf{L}^\frown = \begin{bmatrix} 0 & \dfrac{\partial\widehat{u}_f}{\partial\widehat{k}} & 0 \\ 0 & 0 & 0 \\ 0 & 0 & 0 \end{bmatrix} \tag{9}$$

The current vector $\widehat{\mathbf{J}}$ can be defined as

$$\widehat{\mathbf{J}} = \widehat{\sigma}\left(\widehat{\mathbf{E}} + \widehat{\mathbf{V}}\times\widehat{\mathbf{B}}\right), \tag{10}$$

In the absence of applied electricity and considering the influence of transverse magnetic field such that $\widehat{\mathbf{B}} = (0, B_0, 0)$. Then above equation becomes

$$\widehat{\mathbf{J}}\times\widehat{\mathbf{B}} = \left(-\widehat{\sigma}B_0^2\widehat{u}_f, 0, 0\right) \tag{11}$$

Invoking the velocity components of both phases and performing essential mathematical manipulation, then the main governing equations in components form are given as

$$\frac{\partial\widehat{u}_f}{\partial\widehat{x}} = 0. \tag{12}$$

$$\frac{\partial}{\partial\widehat{k}}\left(\frac{\widehat{\mu}_s}{1+\widehat{\lambda}_1}\frac{\partial\widehat{u}_f}{\partial\widehat{k}}\right) - \frac{\widehat{s}\widehat{C}}{\left(1-\widehat{C}\right)}\left(\widehat{u}_p - \widehat{u}_f\right) - \frac{\widehat{\sigma}\widehat{B}_0^2\widehat{u}_f}{\left(1-\widehat{C}\right)} = \frac{\partial\widehat{p}}{\partial\widehat{x}}. \tag{13}$$

$$\frac{\partial\widehat{\mu}_p}{\partial\widehat{x}} = 0. \tag{14}$$

$$-\widehat{C}\frac{\partial\widehat{p}}{\partial\widehat{x}} + \widehat{s}\widehat{C}\left(\widehat{u}_p - \widehat{u}_f\right) = 0, \tag{15}$$

$$\frac{\partial}{\partial\widehat{y}}\left(\widehat{k}\frac{\partial\widehat{T}}{\partial\widehat{y}}\right) + \frac{\widehat{\mu}_s}{1+\widehat{\lambda}_1}\left(\frac{\partial\widehat{u}_f}{\partial\widehat{y}}\right)^2 + \frac{16\sigma^*}{3k_1}\frac{\partial^2\widehat{T}}{\partial\widehat{y}^2} = 0. \tag{16}$$

To normalize the flow dynamics, we define the following dimensionless variables and quantities:

Using Eq. (17) in Eqs. (12)–(16), we get the following dimensionless equations:

$$\frac{\partial u_f^*}{\partial x^*} = 0, \tag{18}$$

$$\frac{\partial u_p^*}{\partial x^*} = 0, \tag{19}$$

$$\frac{\partial}{\partial y^*}\left(\frac{\mu_s^*}{1+\widehat{\lambda}_1}\frac{\partial u_f^*}{\partial y^*}\right) - \frac{\widehat{C}}{m^\frown\left(1-\widehat{C}\right)}\left(u_p^* - u_f^*\right) - \frac{\widehat{M}^2}{\left(1-\widehat{C}\right)}u_f^* + \widehat{p} = 0, \tag{20}$$

$$u_p^* - u_f^* = -m^\frown\widehat{p}, \tag{21}$$

$$\frac{\partial}{\partial y^*}\left(k^*\frac{\partial T^*}{\partial y^*}\right) + \frac{\mu_s^*}{1+\widehat{\lambda}_1}\widehat{B}_r\left(\frac{\partial u_f^*}{\partial y^*}\right)^2 + \widehat{R}_{\widehat{d}}\frac{\partial^2 T^*}{\partial y^{*2}} = 0. \tag{22}$$

3. Source of thermal radiated multi-phase flow

Three most famous sources are taken into account, which causes fundamental multi-phase flows with heat transfer:

3.1. Pressure driven multi-phase flow

It is considered that multi-phase flow with heat transfer is mainly, due to the contribution of the constant pressure gradient. This can only be achieved when both walls of the channel are at a stationary position, as shown in Fig. 1. Using Eq. (21) in Eq. (20) yields and performing necessary manipulation in Eq. (22) leads the following set of equations

$$\frac{\partial^2 u_f^*}{\partial y^{*2}} - \frac{\widehat{M}^2\left(1+\widehat{\lambda}_1\right)}{1-\widehat{C}}u_f^* + \frac{\widehat{p}\left(1+\widehat{\lambda}_1\right)}{1-\widehat{C}} = 0. \tag{23}$$

$$\left(1+\widehat{R}_{\widehat{d}}\right)\frac{\partial^2 T^*}{\partial y^{*2}} + \frac{\widehat{B}_r}{1+\widehat{\lambda}_1}\left(\frac{\partial u_f^*}{\partial y^*}\right)^2 = 0. \tag{24}$$

Dimensionless boundary conditions are:

$$u_f^*(y^* = -1) = 0, \qquad u_f^*(y^* = 1) = 0. \tag{25}$$

$$T^*(y^* = -1) = 0, \qquad T^*(y^* = 1) = 1. \tag{26}$$

3.2. Moving wall driven multi-phase flow

Now, it is considered that heated multi-phase flow between flat plates is due to the motion of the upper wall, which moves with the constant velocity U, depicted in Fig. 2. On the other hand, the contribution of a constant pressure gradient is a negligible and lower plate of the channel is still at rest. In view of the above assumptions, the momentum equation along with the boundary condition in the dimensionless form is
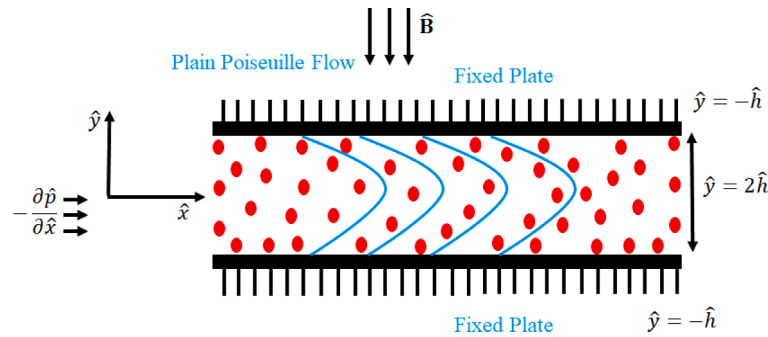
$$u_f^* = \frac{\widehat{u}_{\widehat{f}}}{U}, u_p^* = \frac{\widehat{u}_{\widehat{p}}}{U}, \mu_s^* = \frac{\widehat{\mu}_{\widehat{s}}}{\mu_0}, y^* = \frac{\widehat{y}}{h}, x^* = \frac{\widehat{x}}{h}, k^* = \frac{\widehat{k}}{k_0}, p^* = \frac{\widehat{h}\,\widehat{p}}{\mu_0 U}, T^* = \frac{\widehat{T}-\widehat{T}_0}{\widehat{T}_1-\widehat{T}_0}, \widehat{P} = -\frac{\partial p^*}{\partial x^*}, \widehat{M} = \sqrt{\frac{\widehat{\sigma}}{\mu_0}}\widehat{h}\widehat{B}_0, m = \frac{\mu_0}{\widehat{h}^2\widehat{S}}, \widehat{B}_{\widehat{r}} = \frac{\mu_0 U^2}{k_0\left(\widehat{T}_1-\widehat{T}_0\right)}, \widehat{R}_{\widehat{d}} = \frac{16\sigma^*}{3k_1 k_0} \tag{17}$$

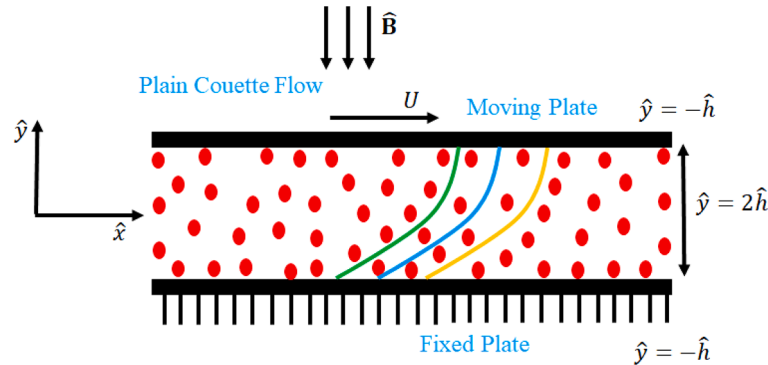**Fig. 1.** Geometry of plane Poiseuille flow.
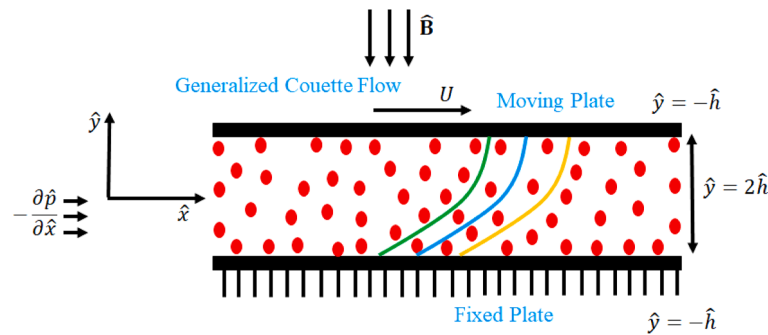

Fig. 2. Geometry of plane Couette flow.

Fig. 3: Geometry of Generalized Couette Flow.

Fig. 3. Geometry of generalized Couette flow.

$$\frac{\partial^2 u_f^*}{\partial y^{*2}} - \frac{\left(1 + \widehat{\lambda}_1\right)\widehat{M}^2}{1 - \widehat{C}} u_f^* = 0, \tag{27}$$

$$u_f^*(y^* = -1) = 0, \qquad u_f^*(y^* = 1) = 1. \tag{28}$$

However, the thermal equation, along with the boundary conditions, will not be disturbed.

3.3. Pressure and moving wall driven multi-phase flow

Many mechanical multi-phase flows obey the mechanism moving wall and constant pressure gradient. In this connection, it is assumed that the bi-phase flow of Jeffrey fluid with heat transfer is due to the upper moving wall incorporated with constant pressure gradient to be seen in Fig. 3.

4. Method of solution

4.1. Pressure driven multi-phase flow

One can see that Eqs. (23) and (24) are linear and coupled differential equations. So, an exact solution subject to boundary conditions Eqs. (25) and (26) is achieved. Then velocity and thermal transport of fluid phase is given as

$$u_f^* = A_1 \left(\cosh\left(\widehat{M} \sqrt{\frac{\left(1 + \widehat{\lambda}_1\right)}{\left(1 - \widehat{C}\right)}} \right) y^* + \sinh\left(\widehat{M} \sqrt{\frac{\left(1 + \widehat{\lambda}_1\right)}{\left(1 - \widehat{C}\right)}} \right) y^* \right)$$

$$+ A_2 \left(\cosh\left(\widehat{M} \sqrt{\frac{\left(1 + \widehat{\lambda}_1\right)}{\left(1 - \widehat{C}\right)}} \right) y^* - \sinh\left(\widehat{M} \sqrt{\frac{\left(1 + \widehat{\lambda}_1\right)}{\left(1 - \widehat{C}\right)}} \right) y^* \right) + \frac{\widehat{p}}{\widehat{M}^2} \tag{29}$$

$$T^* = B_{10} + y^* B_{11} + B_{12} y^{*2} + B_{13} \cosh\left(2\widehat{M}\sqrt{\frac{\left(1+\widehat{\lambda}_1\right)}{\left(1-\widehat{C}\right)}}\right) y^*$$

$$+ B_{14} \sinh\left(2\widehat{M}\sqrt{\frac{\left(1+\widehat{\lambda}_1\right)}{\left(1-\widehat{C}\right)}}\right) y^*. \tag{30}$$

Where, $A_1, A_2, B_{10}, B_{11}, \quad B_{12}$ and B_{14} etc. are some constants which can be determined by following routine calculations given in the appendix.

4.2. Moving wall driven multi-phase flow

The momentum of two-phase Jeffrey fluid which transfer heat under the effects of radiation are:

$$u_f^* = A_3 \left(\cosh\left(\widehat{M}\sqrt{\frac{\left(1+\widehat{\lambda}_1\right)}{\left(1-\widehat{C}\right)}}\right) y^* + \sinh\left(\widehat{M}\sqrt{\frac{\left(1+\widehat{\lambda}_1\right)}{\left(1-\widehat{C}\right)}}\right) y^*\right)$$

$$+ A_4 \left(\cosh\left(\widehat{M}\sqrt{\frac{\left(1+\widehat{\lambda}_1\right)}{\left(1-\widehat{C}\right)}}\right) y^* - \sinh\left(\widehat{M}\sqrt{\frac{\left(1+\widehat{\lambda}_1\right)}{\left(1-\widehat{C}\right)}}\right) y^*\right), \tag{31}$$

$$T^* = B_{20} + y^* B_{21} + B_{22} y^{*2} + B_{23} \cosh\left(2\widehat{M}\sqrt{\frac{\left(1+\widehat{\lambda}_1\right)}{\left(1-\widehat{C}\right)}}\right) y^*$$

$$+ B_{24} \sinh\left(2\widehat{M}\sqrt{\frac{\left(1+\widehat{\lambda}_1\right)}{\left(1-\widehat{C}\right)}}\right) y^*. \tag{32}$$

4.3. Pressure and moving wall driven multi-phase flow

$$u_f^* = A_5 \left(\cosh\left(\widehat{M}\sqrt{\frac{\left(1+\widehat{\lambda}_1\right)}{\left(1-\widehat{C}\right)}}\right) y^* + \sinh\left(\widehat{M}\sqrt{\frac{\left(1+\widehat{\lambda}_1\right)}{\left(1-\widehat{C}\right)}}\right) y^*\right)$$

$$+ A_6 \left(\cosh\left(\widehat{M}\sqrt{\frac{\left(1+\widehat{\lambda}_1\right)}{\left(1-\widehat{C}\right)}}\right) y^* - \sinh\left(\widehat{M}\sqrt{\frac{\left(1+\widehat{\lambda}_1\right)}{\left(1-\widehat{C}\right)}}\right) y^*\right) + \frac{\widehat{p}}{\widehat{M}^2} \tag{33}$$

$$T^* = B_{30} + B_{31} y^* + B_{32} y^{*2} + B_{33} \cosh\left[2\widehat{M}\sqrt{\frac{\left(1+\widehat{\lambda}_1\right)}{\left(1-\widehat{C}\right)}} y^*\right]$$

$$+ B_4 \sinh\left[2\widehat{M}\sqrt{\frac{\left(1+\widehat{\lambda}_1\right)}{\left(1-\widehat{C}\right)}} y^*\right]. \tag{34}$$

5. Results and discussion

The physical interpretation of the results is elaborated in this section. Figs. 4 to 18 are sketched to capture the variations in velocity and temperature distribution for various emerging parameters, namely Hartmann number$(\widehat{M})$, metallic particle concentration$(\widehat{C})$, non-Newtonian parameter or Jeffrey fluid parameter$(\widehat{\lambda}_1)$, Radiation parameter $(\widehat{R_d})$ and Brinkman number$(\widehat{B_r})$. A detailed discussion is made based on three multi-phase flows which cause the heat transfer has been elaborated in segregated subsections:

5.1. Pressure driven multi-phase Flow

Figs. 4 to 8 are prepared to examine the different emerging parameters effects on the Jeffrey-Hafnium bi-phase flow and temperature profile. Fig. 4 shows variations inflow for different values of Hartmann number. The diagram depicts that bi-phase flow gradually reduces its momentum. It holds physically as an increase in values of Hartmann number yields enhancement in Lorentz force. Lorentz force introduces a resistive force which hampers the fluid flow. Therefore, the velocity field decreases. Fig. 5 exhibits the variations in flow for metallic particle concentration. It is noticed that the addition of metallic particles in the base fluid increases the momentum of multi-phase flow as predicted in [19] for non-Newtonian fluid bi-phase flow. Similarly, the velocity of fluid enhances subject to Jeffrey fluid parameter in Fig. 6. Higher values in non-Newtonian fluid parameter cause shear-thinning effects. In addition to this, heating effects at the upper wall, further, attenuates the viscosity of the base liquid. Therefore, velocity increases during the process. Effects of radiation on thermal profile are shown in Fig. 7. The radiation parameter defines the relative contribution of conduction heat transfer to thermal radiation transfer. It is obvious from that heat transfer rate is enhancing, which leads to a decline in thermal profile against the dimensionless parameter. Quite the opposite trend in the behavior of thermal profile is observed against Brinkman number in Fig. 8. The temperature of bi-phase flow increases with respect to Brinkman number, which states that viscous dissipation effects are more prominent. These effects increase the heat generation within the fluid, and hence the temperature of fluid enhances [6].
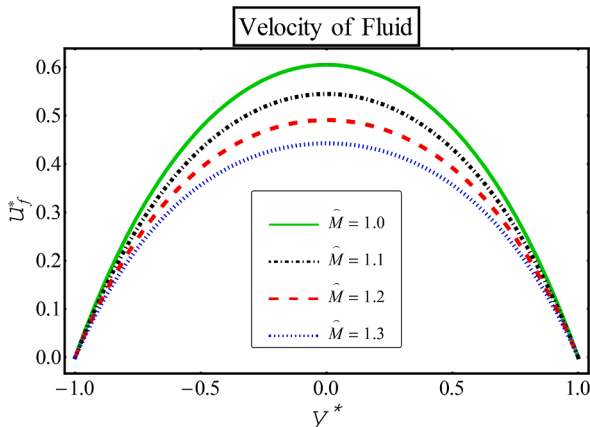
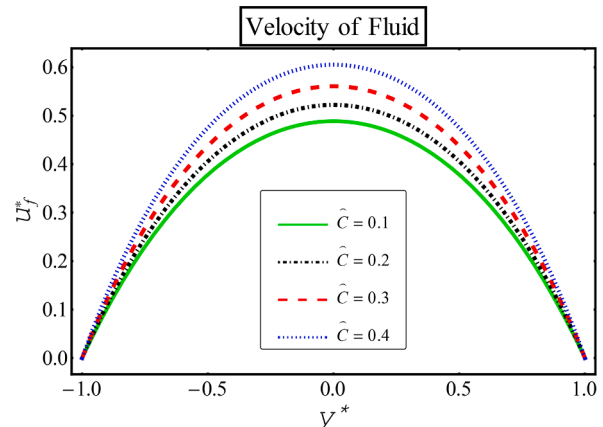**Fig. 4.** Variations in flow and temperature for Hartmann number.

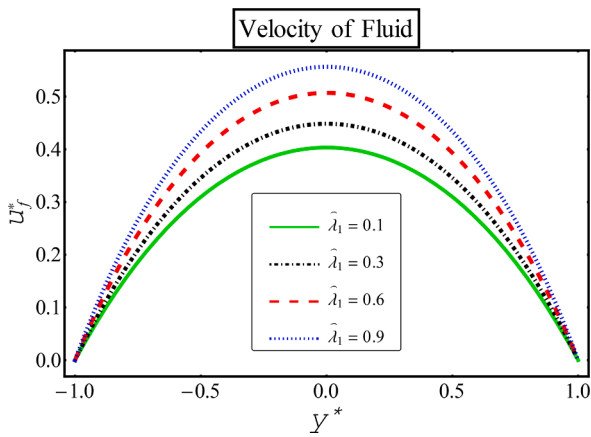**Fig. 5.** Variations in flow and temperature for metallic particles concentration.

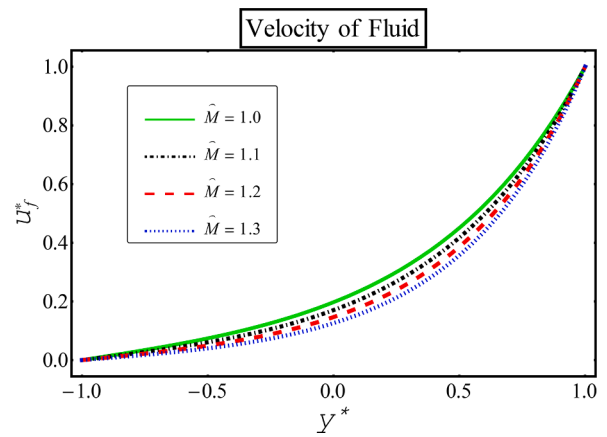**Fig. 6.** Variations in flow and temperature for the non-Newtonian parameter.
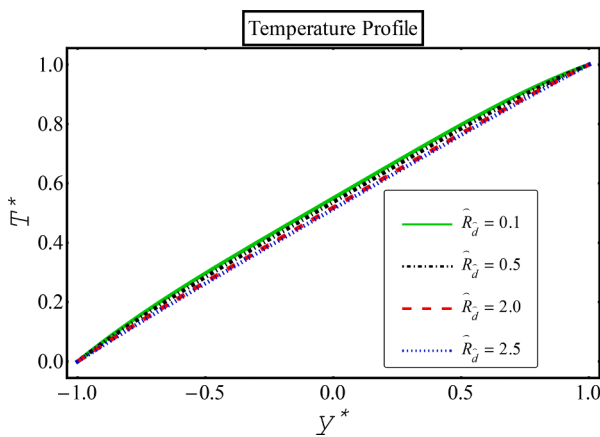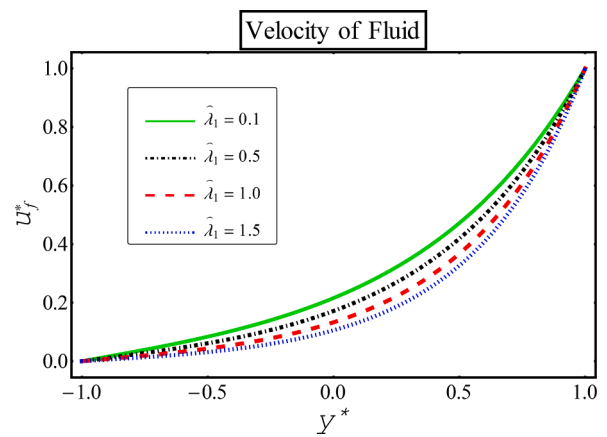

Fig. 7. Variations in temperature for Radiation parameter.

Fig. 8. Variations in temperature for Brinkman number.

Fig. 9. Variations inflow for Hartmann number.

Fig. 10. Variations in flow and temperature for the non-Newtonian parameter.
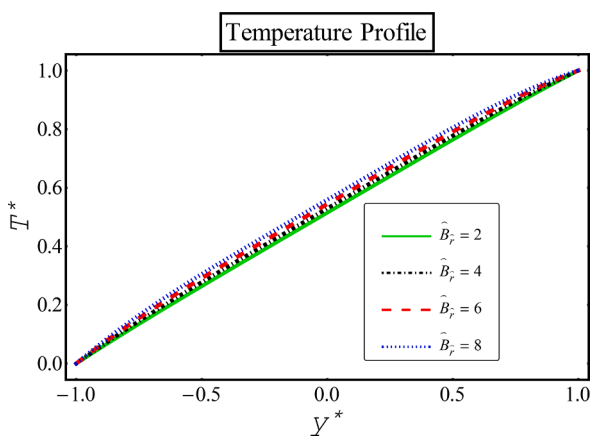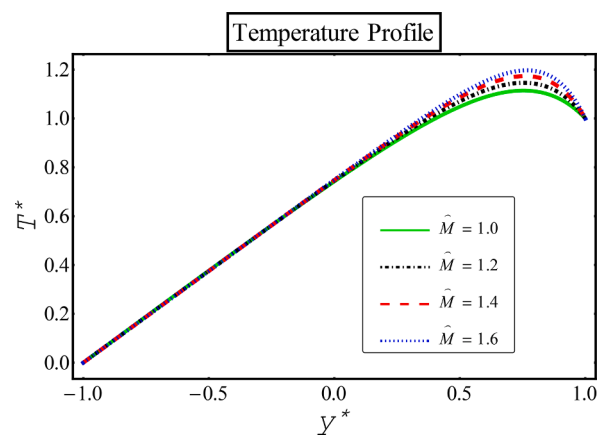

Fig. 11. Variations in flow and temperature for Hartmann number.

5.2. Moving wall driven multi-phase flow

In Figs. 9–13, we examine the role of emerging parameters on the velocity and heat transfer of multi-phase Jeffrey fluid flow which caused by merely, due to the constant motion of the upper heated wall. Fig. 9 is plotted versus Hartmann number. The variation of magnetic field intensity resists the motion of the Jeffrey-Hafnium flow. This reduction in the velocity is caused by the factor which is stated in the previous case. Unlike, the pressure-driven multi-phase flow the velocity declines for Jeffrey fluid parameter. From Fig. 10, it is observed that by increasing

the non-Newtonian parameter velocity decreases. Contribution of Hartmann number is given in Fig. 11. It is evident from the fact that increase in Hartmann number reduces the velocity of the fluid. This retardation increases the force of friction between fluid particles and fluid layers which adds more energy in the system. It is very interesting to note that the effects of Hartmann number on thermal profile are only, significant and evident near the upper wall. However, the overall behavior of Brinkman number and radiation parameter on temperature is the same as for the previous case, as shown in Figs. 12 and Fig. 13, respectively.
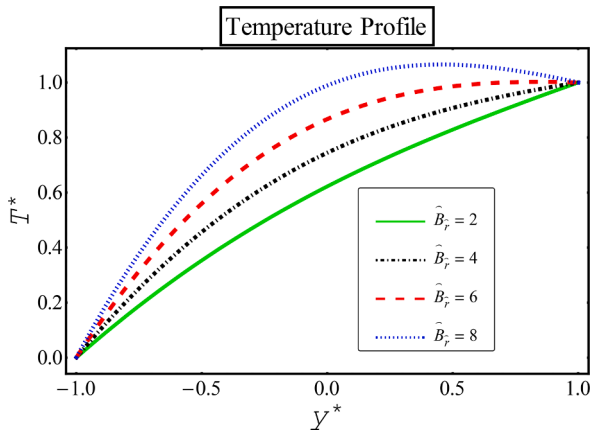
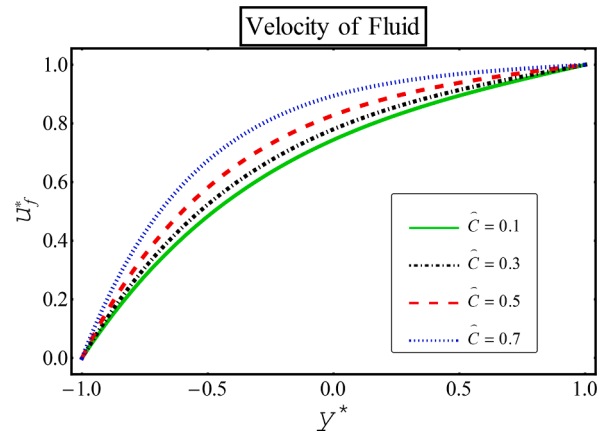**Fig. 12.** Variations in temperature for Brinkman number.

Fig. 13. Variations in temperature for Radiation parameter.

Fig. 14. Variations in flow and temperature for Hartmann number.

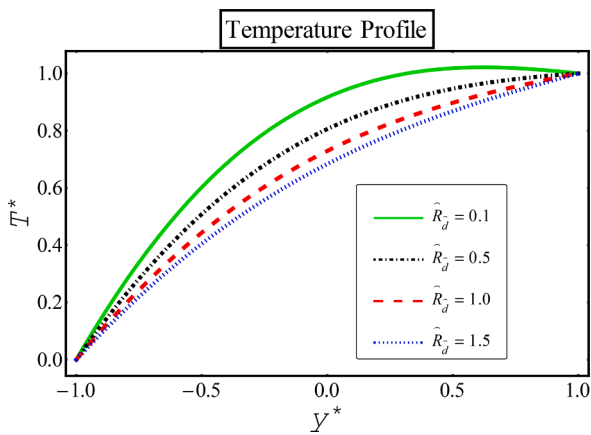**Fig. 15.** Variations in flow and temperature for metallic particles concentration.

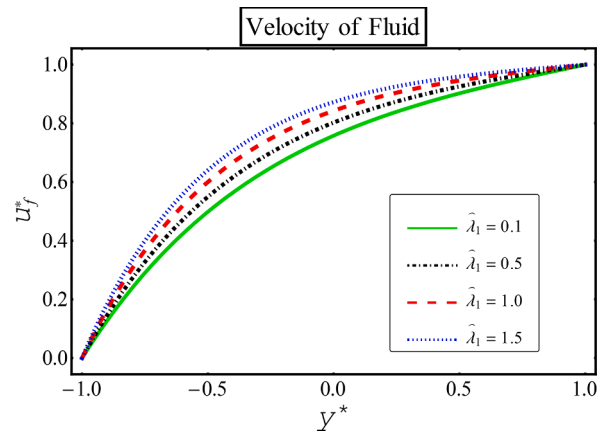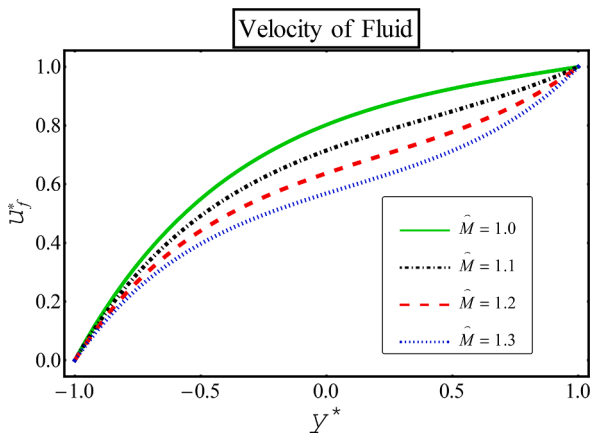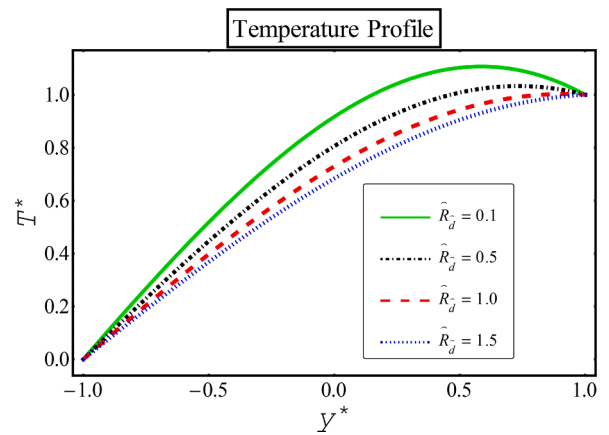**Fig. 16.** Variations in flow and temperature for the non-Newtonian parameter.

Fig. 17. Variations in temperature for Radiation parameter.

5.3. Pressure and moving wall driven multi-phase flow

Finally, this portion describes the velocity and thermal behavior of pressure and moving wall driven multi-phase flow in Figs. 14–18. Fig. 14 shows variations in fluid velocity against Hartmann number. Base liquid reduces in momentum as Hartmann number is enhanced. On the contrary, fluid velocity increases Fig. 15 as the additional metallic particles are incorporated. Similarly, the flow of bi-phase flow speeds up as the Jeffrey fluid parameter is varied in Fig. 16. Increase in non-Newtonian parameter brings shear-thinning effects which allow fluid to move

fast. Finally, energy gradually expunges for an increase in radiation parameters, as shown in Fig. 17. Nonetheless, temperature profile increases due to with respect to increasing the Brinkman number in Fig. 18.

6. Concluding Remarks

Two-phase flows of non-Newtonian fluid with heat transfer through the horizontal channel are investigated. Jeffrey fluid is taken as a base
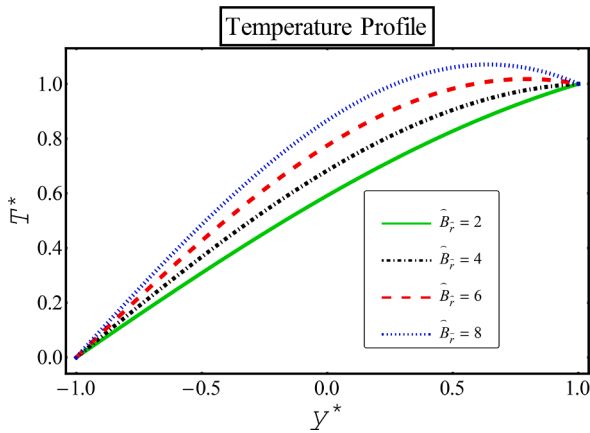
Fig. 18. Variations in temperature for Brinkman number.

liquid which suspended with spherical Hafnium particles. The magnetic field in transverse direction is applied along with the impact of radiation. An exact solution is obtained for each multi-phase flow. A detailed parametric study is carried out, and the main outcomes of this investigation are:

- The momentum of multi-phase flow decreases in each case against the Hartmann number.
- Jeffrey fluid parameter has a different impact on the velocity of base fluid for wall driven multi-phase flow.

- The radiation parameter declines temperature distribution for all types of flow.
- More energy adds to the system due to the Brinkman number.
- Jeffrey multi-phase flow reduces back to Newtonian multi-phase for $\widehat{\lambda}_1 \to 0$.

Compliance with Ethical Standards

No funding was received.

Credit author statement

Component of the research Author's number, substantial contribution to conception and design Mubbashar Nazeer, substantial contribution to acquisition of data Farooq Hussain, substantial contribution to analysis and interpretation of data M. Ozair Ahmad and Sadia Saeed, revised drafting the article Yu-Ming Chu and Seifefine Kadry, critically revising the article for important intellectual content M. Ijaz Khan, final approval of the version to be published by All authors.

Declaration of Competing Interest

The authors have no conflict of interest related to this manuscript.

Acknowledgements

Appendix

.

$$A_1 = A_2 = -\frac{\widehat{p}\,Sech\left(\widehat{M}\sqrt{\dfrac{1+\widehat{\lambda}_1}{1-\widehat{C}}}\right)}{2\widehat{M}^2}, \qquad B_{10} = \frac{1}{2} - B_2 - \cosh\left[2\widehat{M}\sqrt{\dfrac{1+\widehat{\lambda}_1}{1-\widehat{C}}}\right]B_3,$$

$$B_{11} = \frac{1}{2}\left(1 - 2\sinh\left[2\widehat{M}\sqrt{\dfrac{1+\widehat{\lambda}_1}{1-\widehat{C}}}\right]B_4\right), \qquad B_{12} = \frac{\widehat{M}^2\left(\dfrac{1+\widehat{\lambda}_1}{1-\widehat{C}}\right)Br A_1 A_2}{(1+Rd)\left(1+\widehat{\lambda}_1\right)},$$

$$B_{22} = \frac{\widehat{M}^2\dfrac{\left(1+\widehat{\lambda}_1\right)}{(1-C)}Br A_3 A_4}{(1+Rd)\left(1+\widehat{\lambda}_1\right)}, B_{23} = -\frac{Br\left(A_3^2 + A_4^2\right)}{4(1+Rd)\left(1+\widehat{\lambda}_1\right)}, B_{24} = \frac{Br\left(-A_3^2 + A_4^2\right)}{4(1+Rd)\left(1+\widehat{\lambda}_1\right)},$$

$$A_5 = \frac{1}{4}\left(Csch\left[\widehat{M}\sqrt{\dfrac{\left(1+\widehat{\lambda}_1\right)}{\left(1-\widehat{C}\right)}}\right] + Sech\left[\widehat{M}\sqrt{\dfrac{\left(1+\widehat{\lambda}_1\right)}{\left(1-\widehat{C}\right)}}\right] - \frac{2\dfrac{P\left(1+\widehat{\lambda}_1\right)}{(1-\widehat{C})}Sech\left[\widehat{M}\sqrt{\dfrac{\left(1+\widehat{\lambda}_1\right)}{(1-\widehat{C})}}\right]}{\widehat{M}^2\dfrac{\left(1+\widehat{\lambda}_1\right)}{(1-\widehat{C})}}\right),$$

$$B_{13} = -\frac{Br\left(A_1^2 + A_2^2\right)}{4(1+Rd)\left(1+\widehat{\lambda}_1\right)}, B_{14} = \frac{Br\left(-A_1^2 + A_2^2\right)}{4(1+Rd)\left(1+\widehat{\lambda}_1\right)},$$

$$A_3 = \frac{1}{4}\left(Csch\left[\widehat{M}\sqrt{\dfrac{\left(1+\widehat{\lambda}_1\right)}{\left(1-\widehat{C}\right)}}\right] + Sech\left[\widehat{M}\sqrt{\dfrac{\left(1+\widehat{\lambda}_1\right)}{\left(1-\widehat{C}\right)}}\right]\right),$$

$$A_4 = \frac{1}{4}\left(-Csch\left[\widehat{M}\sqrt{\frac{\left(1+\widehat{\lambda}_1\right)}{\left(1-\widehat{C}\right)}}\right] + Sech\left[\widehat{M}\sqrt{\frac{\left(1+\widehat{\lambda}_1\right)}{\left(1-\widehat{C}\right)}}\right]\right),$$

$$B_{20} = \frac{1}{2} - B_{21} - \cosh\left[2\widehat{M}\sqrt{\frac{\left(1+\widehat{\lambda}_1\right)}{\left(1-\widehat{C}\right)}}\right]B_{23}, \quad B_{21} = \frac{1}{2}\left(1 - 2\sinh\left[2\widehat{M}\sqrt{\frac{\left(1+\widehat{\lambda}_1\right)}{\left(1-\widehat{C}\right)}}\right]B_{24}\right),$$

$$A_6 = \frac{1}{4}\left(-Csch\left[\widehat{M}\sqrt{\frac{\left(1+\widehat{\lambda}_1\right)}{\left(1-\widehat{C}\right)}}\right] + Sech\left[\widehat{M}\sqrt{\frac{\left(1+\widehat{\lambda}_1\right)}{\left(1-\widehat{C}\right)}}\right] - \frac{2\frac{P\left(1+\widehat{\lambda}_1\right)}{\left(1-\widehat{C}\right)}Sech\left[\widehat{M}\sqrt{\frac{\left(1+\widehat{\lambda}_1\right)}{\left(1-\widehat{C}\right)}}\right]}{\widehat{M}^2\frac{\left(1+\widehat{\lambda}_1\right)}{\left(1-\widehat{c}\right)}}\right),$$

$$B_{30} = \frac{1}{2} - B_{32} - \cosh\left[2\widehat{M}\sqrt{\frac{\left(1+\widehat{\lambda}_1\right)}{\left(1-\widehat{C}\right)}}\right]B_{33}, \quad B_{31} = \frac{1}{2}\left(1 - 2\sinh\left[2\widehat{M}\sqrt{\frac{\left(1+\widehat{\lambda}_1\right)}{\left(1-\widehat{C}\right)}}\right]B_{34}\right),$$

$$B_{32} = \frac{\widehat{M}^2\frac{\left(1+\widehat{\lambda}_1\right)}{\left(1-\widehat{C}\right)}BrA_5A_6}{\left(1+Rd\right)\left(1+\widehat{\lambda}_1\right)}, B_{33} = -\frac{Br\left(A_5^2+A_6^2\right)}{4\left(1+Rd\right)\left(1+\widehat{\lambda}_1\right)}, B_{34} = \frac{Br\left(-A_5^2+A_6^2\right)}{4\left(1+Rd\right)\left(1+\widehat{\lambda}_1\right)}.$$

References

[1] N. Dalir, Numerical study of entropy generation for forced convection flow and heat transfer of a Jeffrey fluid over a stretching sheet, Alex Eng. J. 53 (4) (2014) 769–778.

[2] M.M Bhatti, A. Zeeshan, Analytic study of heat transfer with variable viscosity on solid particle motion in dusty Jeffery fluid, Mod. Phys. Lett. B 30 (16) (2016), 1650196.

[3] R Ellahi, F Hussain, A Zeeshan, K Vafai, Modelling study on heated couple stress fluid peristaltically conveying gold nanoparticles through coaxial tubes: A remedy for gland tumors and arthritis, J. Mol. Liq. 268 (2018) 149–155, https://doi.org/10.1016/j.molliq.2018.07.034.

[4] S.U Rahman, R Ellahi, S Nadeem, Q.M.Z. Zia, Simultaneous effects of nanoparticles and slip on Jeffrey fluid through tapered artery with mild stenosis, J. Mol. Liq. 218 (1) (2016) 484–493.

[5] R. Ellahi, F. Hussain, F. Ishtiaq, A. Hussain, Peristaltic transport of Jeffrey fluid in a rectangular duct through a porous medium under the effect of partial slip: An application to upgrade industrial sieves/filters, Pramana (J. Phys.) 93 (34) (2019), https://doi.org/10.1007/s12043-019-1781-8.

[6] K. Ramesh, Effects of viscous dissipation and Joule heating on the Couette and Poiseuille flows of a Jeffrey fluid with slip boundary conditions, J. Propul. Power Res. 7 (4) (2018) 329–341.

[7] F.M. Abbasi, S.A. Shehzad, T. Hayat, M.S. Alhuthali, Mixed convection flow of Jeffrey nanofluid with thermal radiation and double stratification, J. Hydrody. 28 (5) (2016) 840–849.

[8] S.A. Shehzad, Z. Abdullah, A. Alsaedi, F.M. Abbasi, T. Hayat, Thermally radiative three-dimensional flow of Jeffrey nanofluid with internal heat generation and magnetic field, J. Magn. Magn. Mater. 397 (1) (2015) 108–114.

[9] M. Turkyilmazoglu, I. Pop, Exact analytical solutions for the flow and heat transfer near the stagnation point on a stretching/shrinking sheet in a Jeffrey fluid, Int. J. Heat Mass Tran. 57 (1) (2013) 82–88.

[10] R. Ellahi, S.U. Rahman, S. Nadeem, Blood flow of Jeffrey fluid in a catherized tapered artery with the suspension of nanoparticles, Phys. Lett. A 378 (4) (2014) 2973–2980.

[11] R. Ellahi, F. Hussain, Simultaneous effects of MHD and partial slip on peristaltic flow of Jeffrey fluid in a rectangular duct, J. Magn. Magn. Mater. 393 (2015) 284–292.

[12] M. Nazeer, F. Hussain, Q. Shahzad, Z. Ali, S. Kadry, M.Y. Chu, Computational study of solid-liquid supercritical flow of 4th grade fluid through magnetized surface, Pysica Sripta 96 (1) (2020) doi———.

[13] A. Zeeshan, Z. Ali, R.M. Gourji, F. Hussain, S. Nadeem, Flow analysis of bi-convective heat and mass transfer of two-dimensional couple stress fluid over a paraboloid of revolution, Int. J. Modern Phys. B (2020), https://doi.org/10.1142/S0217979220501106.

[14] R. Ellahi, A. Zeeshan, F. Hussain, T. Abbas, Two-phase couette flow of couple stress fluid with temperature dependent viscosity thermally affected by magnetized moving surface, Symmetry 11 (5) (2019) 647–660.

[15] A. Zeeshan, F. Hussain, R. Ellahi, K. Vafai, A study of gravitational and magnetic effects on coupled stress bi-phase liquid suspended with crystal and Hafnium particles down in steep channel, J. Mol. Liq. 286 (2019), 110898.

[16] M. Nazeer, F. Hussain, Q. Shahzad, I.M. Khan, S. Kadry, M.Y. Chu, Perturbation solution of multi-phase flows of Third grade dispersions suspended with Hafnium and crystal particles, Surf. Interfaces (2020), https://doi.org/10.1016/j.surfin.2020.100803.

[17] S.M. Atif, S. Hussain, M. Sagheer, Heat and mass transfer analysis of time-dependent tangent hyperbolic nanofluid flow past a wedge, Phys. Lett. A 383 (11) (2019) 1187–1198.

[18] M.Y. Chu, M. Nazeer, F. Hussain, I.M. Khan, H. Rafi, S. Qayyum, Z. Abdelmalek, Combined effects of heat source/sink, radiative heat flux, temperature dependent thermal conductivity on forced convective Rabinowitsch fluid, Int. Commun. Heat Mass Trans. (2020), https://doi.org/10.1016/j.icheatmasstransfer.2020.105011.

[19] M Nazeer, N Ali, F Ahmad, M Latif, Numerical and perturbation solutions of third-grade fluid in a porous channel: boundary and thermal slip effects, Pramana – J. Phys. 94 (1) (2020) 44.

[20] R. Ellahi, A. Zeeshan, F. Hussain, T. Abbas, Thermally charged MHD bi-phase flow coatings with non-Newtonian nanofluid and Hafnium particles along slippery walls, Coatings 9 (5) (2019) 300–313.

[21] M.M. Bhatti, R. Ellahi, A. Zeeshan, M. Marin, N. Ijaz, Numerical study of heat transfer and Hall current impact on peristaltic propulsion of particle-fluid suspension with compliant wall properties, Mod. Phys. Lett. B (2019), 1950439.

[22] M.M. Bhatti, A. Shahid, T. Abbas, S.Z. Alamri, R. Ellahi, Study of activation energy on the movement of gyrotactic microorganism in a magnetized nanofluids past a porous plate, Processes 8 (2020) 328–348.

[23] T.N. Thoi, M.M. Bhatti, J.A. Ali, S.M. Hamad, M. Sheikholeslami, A. Shafee, R. Haq, Analysis on the heat storage unit through a Y-shaped fin for solidification of NEPCM, J. Mol. Liq. 292 (2019), 111378.

[24] L. Zhang, M.M. Bhatti, M. Marin, K.S. Mekheimer, Entropy analysis on the blood flow through anisotropically tapered arteries filled with magnetic Zinc-Oxide (ZnO) nanoparticles, Entropy 22 (2020) 1070.

[25] M. Nazeer, F. Ahmad, A. Saleem, M. Saeed, S. Naveed, M. Shaheen, E. Al Aidarous, Effects of constant and space-dependent viscosity on eyring–powell fluid in a pipe: comparison of the perturbation and explicit finite difference methods, Z. Naturforschung A 74 (11) (2019) 961–969.

[26] F. Ahmad, M. Nazeer, M. Saeed, A. Saleem, W. Ali, Heat and mass transfer of temperature-dependent viscosity models in a pipe: effects of thermal radiation and heat generation, Z. Naturforschung A 75 (3) (2020) 225–239, a.

[27] M. Nazeer, F. Ahmad, M. Saeed, A. Saleem, S. Naveed, Z. Akram, Numerical solution for flow of a Eyring–Powell fluid in a pipe with prescribed surface temperature, J. Braz. Soc. Mech. Sci. Eng. 41 (11) (2019) 518–528.

[28] N. Ali, F. Nazeer, M. Nazeer, Flow and heat transfer analysis of an Eyring–Powell fluid in a pipe, Z. Naturforschung A 73 (3) (2018) 265–274, a.

[29] F. Hussain, R. Ellahi, A. Zeeshan, Mathematical models of electro-magnetohydrodynamic multiphase flows synthesis with nano-sized hafnium particles, Appl. Sci. (MDPI) 8 (2018) 275–292.